



OPEN

Energy driven mechanism of surrounding rock deformation and failure of mining roadway and classified control technology

Xuesheng Liu^{1,2,3}, Yu Zhang¹✉, Deyuan Fan^{1,2}✉, Yongqiang Zhao^{1,2}, Yudong Gao¹, Hongxi Pei¹ & Zhihan Shi¹

The energy evolution of surrounding rock under mining influence has a crucial impact on its stability. Taking the I0104₃02 transportation roadway of Shuangma as the engineering background, the energy evolution law of surrounding rock in mining roadway was obtained by FLAC3D. The energy influence range and value of elastic energy and dissipated energy at both sides of the roadway gradually increase with the mining. The energy value at the face end reaches its maximum, with the dissipated energy release area forming a butterfly-shaped distribution and the elastic energy accumulation area forming a trapezoidal accumulation pattern. Subsequently, the surrounding rock of the roadway is divided into energy consumption zone, energy supply zone, and unaffected zone based on the range of two energies. Then, the types of surrounding rock deformation and failure are identified from two aspects: energy level K and energy release rate V. When $K \geq 1$ and $V \geq 1$, the surrounding rock of the roadway undergoes impact instability; when $V < 1$, the surrounding rock of the roadway undergoes large deformation failure. Furthermore, "Multi-Level pressure yielding" and "Relief-Support" control technology are proposed for the two types of failure, and field verification has been carried out in Shuangma and Xinjulong.

Keywords Mining roadway, Energy-driven, Large deformation, Impact instability, Classified control

During the process of underground mineral resource mining, the stress field around the ore body and the filling body will be redistributed, forming a mining stress field¹. With the progress of mining activities, the roadway is not only affected by the original rock stress but also by the mining stress². The complexity, particularity, and variability of the stress environment of the surrounding rock in mining roadway make the deformation and failure of the roadway complex and highly variable.

The deformation and failure of surrounding rock in roadway are considered to be caused by the plastic zones generated by the surrounding rock³. Hermann Kastner⁴ proposed the classic plastic zone theory of surrounding rock in roadway, which laid the theoretical foundation for the study of the failure of surrounding rock in roadway under equal pressure stress fields. Wang et al.⁵ derived the approximate solution of the boundary equation of the plastic zone of surrounding rock in non-equal pressure circular roadway considering the effect of support force, and obtained the influence of support resistance on the range and shape of the plastic zone of surrounding rock in roadway. Guo et al.⁶ theoretically derived the boundary equation of the plastic zone of surrounding rock in circular roadway under non-equal pressure stress conditions and discovered the "butterfly-shaped" irregularity of the plastic zone of surrounding rock in roadway. Hong et al.⁷ studied and found that high-level stress has the greatest impact on the failure of deep roadway. Under high-level stress, the sides of the roadway are severely squeezed, the convergence of both sides increases, the roof and floor are severely deformed, and there is a high possibility of rupture at the arch. Shang et al.⁸ used numerical simulation analysis to determine the cause of roadway instability when the roof rock mass has high strength and the floor has low strength, and summarized the characteristics of deep roadway instability.

In recent years, many experts at home and abroad have conducted in-depth research on the stability of surrounding rock in mining roadway and proposed effective support design schemes. Jing⁹ used the "anchor-

¹College of Energy and Mining Engineering, Shandong University of Science and Technology, Qingdao 266590, China. ²State Key Laboratory of Disaster Prevention and Ecology Protection in Open-pit Coal Mines, Shandong University of Science and Technology, Qingdao 266590, China. ³National Energy Group Ningxia Coal Industry Co, Ltd., Yinchuan 750011, China. ✉email: zy17860658920@163.com; deyuan926@126.com

frame" joint support technology to control the soft and broken roadway, established the "anchor-frame" joint support composite arch model, and calculated the ultimate bearing capacity of this type of structure. Qing et al.¹⁰ starting from the perspective of the surrounding rock's existence of loose and broken zones, deeply analyzed the types of roadway support loads, and based on a large number of research results, established the "loose circle support theory". Daemen¹¹ conducted research on the stability of deep-buried high-stress soft rock roadway, considering the effect of the self-weight of the rock mass in the plastic zone, and established a functional relationship between the surrounding rock and support characteristic curves. Zhang et al.¹² used experimental and numerical simulation methods to compare and analyze the stability of soft rock roadway under the action of steel arch frames and grid steel arch frames, and proposed a reasonable support plan for controlling the large deformation of soft rock. Zhao et al.¹³ analyzed the law of change in the interaction force between roadway surrounding rock and support, and the research results showed that compared with grid steel arch support, the surrounding rock pressure increased by about 80% under the condition of steel arch support.

At present, domestic and foreign scholars generally judge the instability mechanism of failure from the classical elastoplastic strength criteria and analyze the distribution range of surrounding rock failure and targeted support optimization design from the perspective of stress.¹⁴ These research works have a certain reference for guiding the mechanism of deformation and failure of surrounding rock in mining roadway and the stability of surrounding rock in roadway. However, there is not enough in-depth discussion on the energy-driven mechanism of surrounding rock deformation and failure from the perspective of energy, and no classification control technology for surrounding rock deformation and failure has been proposed. Therefore, based on the transportation roadway of the I0104₃02 working face in Shuangma Mine as the engineering background, this paper uses a combination of numerical simulation and field practice to study the energy partition evolution law of surrounding rock in mining roadway, reveal the mechanism of deformation and failure of surrounding rock in mining roadway, construct a type identification of surrounding rock deformation and failure, and propose corresponding surrounding rock deformation control technology, which is verified in combination with engineering practice. The research results are of great practical significance for ensuring the stability of surrounding rock in mining roadway.

Mechanism of deformation and failure of surrounding rock in mining roadway

Law of energy evolution of surrounding rock in mining

Site engineering conditions

The I0104₃02 working face of Shuangma Mine has an inclined length of 266.5 m, a strike length of 1241.4 m, and a burial depth of about 300 m. The coal seam structure is simple, with an average coal seam thickness of about 1.71 m, no intercalations, and belongs to a stable coal seam. The roof of the coal seam is mainly sandstone, with an average thickness of 10.91 m, and the floor is mainly siltstone, with an average thickness of 15.75 m. The physical and mechanical parameters of the coal seam and rock layers are shown in Table 1.

Due to the strong mining pressure manifestations during the mining period, the surrounding rock deformation and failure are abnormal, which seriously affects the normal production of the working face, and the cost and difficulty of repair are high. To prevent this problem from occurring again, it is planned to carry out related research on the transportation roadway of the I0104₃02 working face.

Numerical simulation scheme

Based on the actual engineering geological conditions, the FLAC3D numerical simulation software is used to establish a numerical model. The length, width and height of the model are 600 m, 400 m and 100 m, respectively. In the model, the width and height of working face are 260 m and 2 m, respectively, and those of roadway are both 4 m, as shown in Fig. 1. The model is a free surface on top, with a vertical load of 7.5×10^6 kN applied, and displacement constraints are applied on all sides and bottom, using the Mohr–Coulomb constitutive model.

To explore the impact of mining activities on the energy changes of surrounding rock in roadway at different distances from the working face, the energy of the roof, floor, both sides, and floor rock units of the surrounding rock is monitored. A measuring line is arranged 350 m away from the working face. To eliminate the influence of boundary effects and insufficient mining on the monitoring results, monitoring is started after the working face has retreated 300 m, and then a record is made every 10 m the working face retreats, with a total of 6 groups monitored. The layout of the monitoring surface measuring line is shown in Fig. 2.

Lithology	Density (g/cm ³)	Compressive strength (MPa)	Tensile strength (MPa)	Elastic modulus (GPa)	Poisson ratio	Friction (°)	Cohesion (MPa)
Siltstone	2.6	35.43	4.22	2.78	0.21	37.69	1.08
Fine-grained sandstone	2.2	32.89	2.02	8.92	0.33	63	3.31
Coal	1.3	17.34	1.97	1.34	0.25	32.15	0.34
Siltstone	2.7	35.43	4.22	2.78	0.21	37.69	1.08
Medium-grained sandstone	2.4	58.32	4.22	5.79	0.25	41.51	4.97
Fine-grained sandstone	2.2	32.89	2.02	8.92	0.33	63	3.31

Table 1. The physical and mechanical parameters.

FLAC3D
Version:6.0.60
URL: <https://www.itasca-cg.com/software/FLAC3D>
Visio
Version:2021
URL: <https://www.microsoft.com/en-us/download>

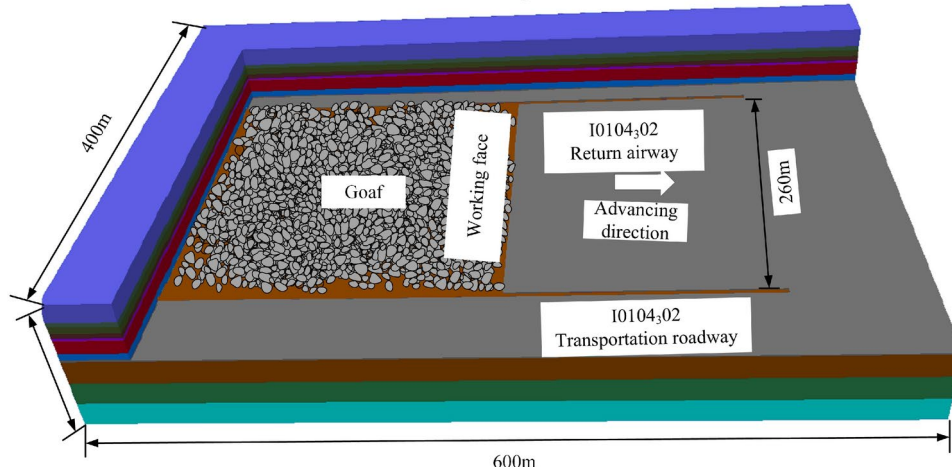


Fig. 1. Numerical simulation model.

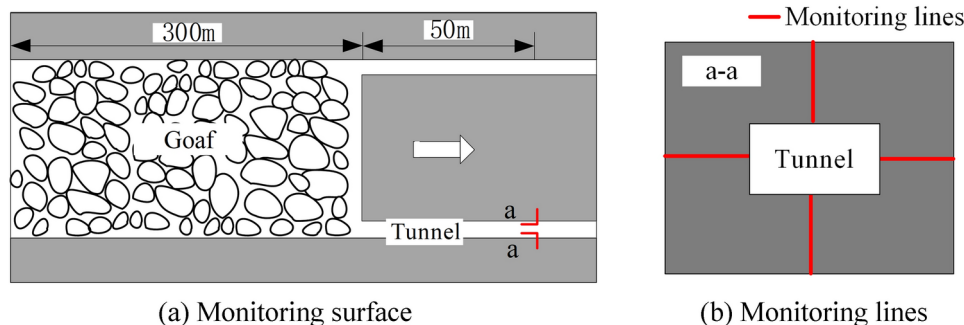


Fig. 2. Monitoring surface and monitoring lines layout.

Simulation results analysis

Before mining, the surrounding rock mass of the roadway is in a state of stress balance. Mining activities will disturb the original relatively balanced geostress field, causing the stress field of the surrounding rock to redistribute and produce stress concentration.¹⁵ The energy field is also like this. The surrounding rock mass is the carrier of energy. When the coal seam is excavated, due to the influence of mining, energy is transmitted and accumulated towards the edge of the roadway. If the elastic energy accumulated in some areas of the surrounding rock exceeds the limit it can bear, it will lead to a surge in dissipated energy of the surrounding rock of the roadway, resulting in plastic deformation or failure.¹⁶ The energy cloud map of the surrounding rock of the roadway is shown in Figs. 3 and 5.

When the working face advances to 30–50 m from the measuring line, the dissipated energy distribution of the surrounding rock of the roadway is mainly butterfly-shaped, symmetrically distributed with the centerline of the roadway as the axis of symmetry, and dissipated energy concentration appears on both sides of the roadway. At this time, the dissipated energy release mainly comes from the stress redistribution after the roadway excavation, and is less affected by mining. When the working face advances to 20 m from the measuring line, the dissipated energy of the surrounding rock of the roadway begins to be affected by mining, and the range of dissipated energy distribution spreads outward. When the working face advances to 10 m from the measuring line, the range of dissipated energy distribution continues to spread outward, and the dissipated energy on both sides of the roadway is significantly increased compared to when the working face advances to 20 m from the measuring line. When the working face advances to the measuring line, the dissipated energy of the surrounding rock of the roadway is no longer symmetrically distributed, and dissipated energy is released at the roof and floor. The dissipated energy release is most affected by mining, and the dissipated energy released by both sides of the roadway reaches its maximum value at this time.¹⁷

In order to explore the impact of the working face advancing to different distances on the range of energy distribution, the dissipated energy monitoring curve of the surrounding rock of the roadway is extracted. The

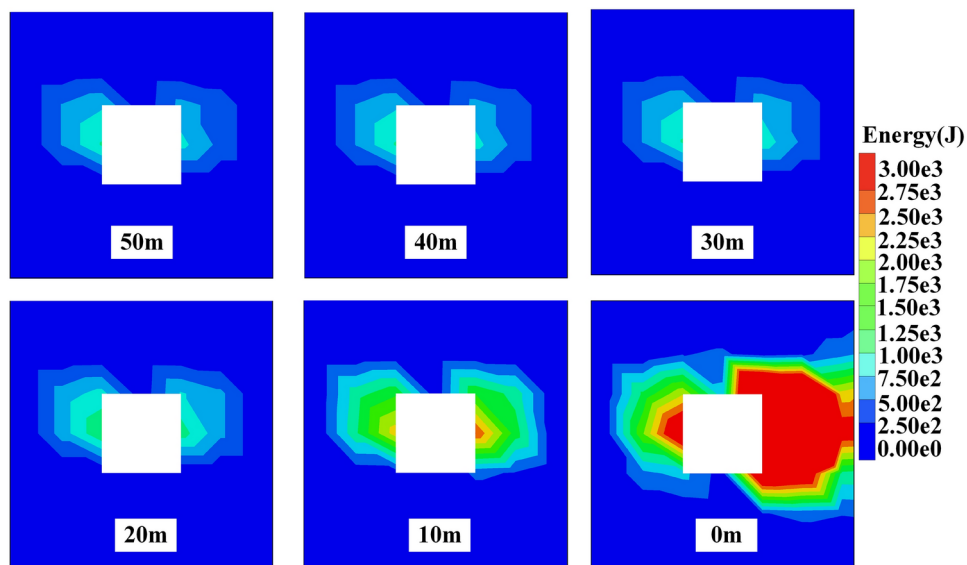


Fig. 3. Dissipated energy distribution of surrounding rock.

dissipated energy distribution curve of the surrounding rock of the roadway at different distances from the working face is shown in Figs. 4 and 6.

According to Fig. 4, when the working face advances to between 30 and 50 m from the measuring line, the dissipated energy distribution boundary on both sides of the roadway is 4 m, and there is no distribution of dissipated energy at the roof and floor. As the working face continues to advance, the range of dissipated energy distribution also gradually expands. When the working face advances to 10 m from the measuring line, the distribution range of dissipated energy on both sides reaches the maximum, of which the solid coal side is about 10 m, and the mining side is about 12 m. When the working face advances to the measuring line, the size of dissipated energy on both sides continues to increase, the range of dissipated energy distribution spreads towards the roof and floor of the roadway, and the distribution boundary distances are 4 m and 6 m, respectively.

When the working face advances to between 30 and 50 m from the measuring line, the distribution of elastic energy of the surrounding rock of the roadway is mainly trapezoidal, symmetrically distributed with the centerline of the roadway as the axis of symmetry. At this time, the accumulation of elastic energy is still the result of stress redistribution, and is less affected by mining. When the working face advances to 20 m from the measuring line, the elastic energy of the surrounding rock of the roadway begins to be affected by mining, and the range of elastic energy distribution spreads outward. When the working face advances to 10 m from the measuring line, the range of elastic energy distribution continues to spread outward, and the elastic energy on both sides of the roadway is significantly increased compared to when the working face advances to 20 m from the measuring line. When the working face advances to the measuring line, the elastic energy of the surrounding rock of the roadway is no longer symmetrically distributed, and elastic energy accumulates at the roof and floor. The accumulation of elastic energy is most affected by mining, and the amount of elastic energy released at the mining side is significantly greater than that at the solid coal side, and the elastic energy accumulated on both sides of the roadway reaches its maximum value at this time.

According to Fig. 6, when the working face advances to between 30 and 50 m from the measuring line, the distribution boundary of elastic energy on both sides of the roadway is 6 m, and there is no distribution of elastic energy at the roof and floor. As the working face continues to advance, the range of elastic energy distribution also gradually expands. When the working face advances to 10 m from the measuring line, the distribution range of elastic energy on both sides reaches the maximum, of which the solid coal side is about 19 m, and the mining side is about 20 m. When the working face advances to the measuring line, the size of elastic energy on both sides continues to increase, the range of elastic energy distribution spreads towards the roof and floor of the roadway, and the distribution boundary distances are 5 m and 9 m, respectively.

From the numerical simulation, it can be known that the advance influence range of the I0104₃02 working face is 30 m. Within the advance influence range, the energy influence range and value at both sides of the roadway gradually increase with the advancement of the working face, and reach the limit at 10 m in advance. The energy influence area spreads from both sides of the roadway towards the roof and floor. The energy value at the head of the working face reaches its maximum, with the dissipated energy release area forming a butterfly-shaped distribution, and the elastic energy accumulation area forming a trapezoidal accumulation pattern, and the range of elastic energy accumulation is greater than the range of dissipated energy release.

Surrounding rock partition model

Research has shown that the accumulation and release of energy are the root causes of deformation and failure of surrounding rock in roadway.¹⁸ Therefore, when the surrounding rock of the roadway deforms and destroys,

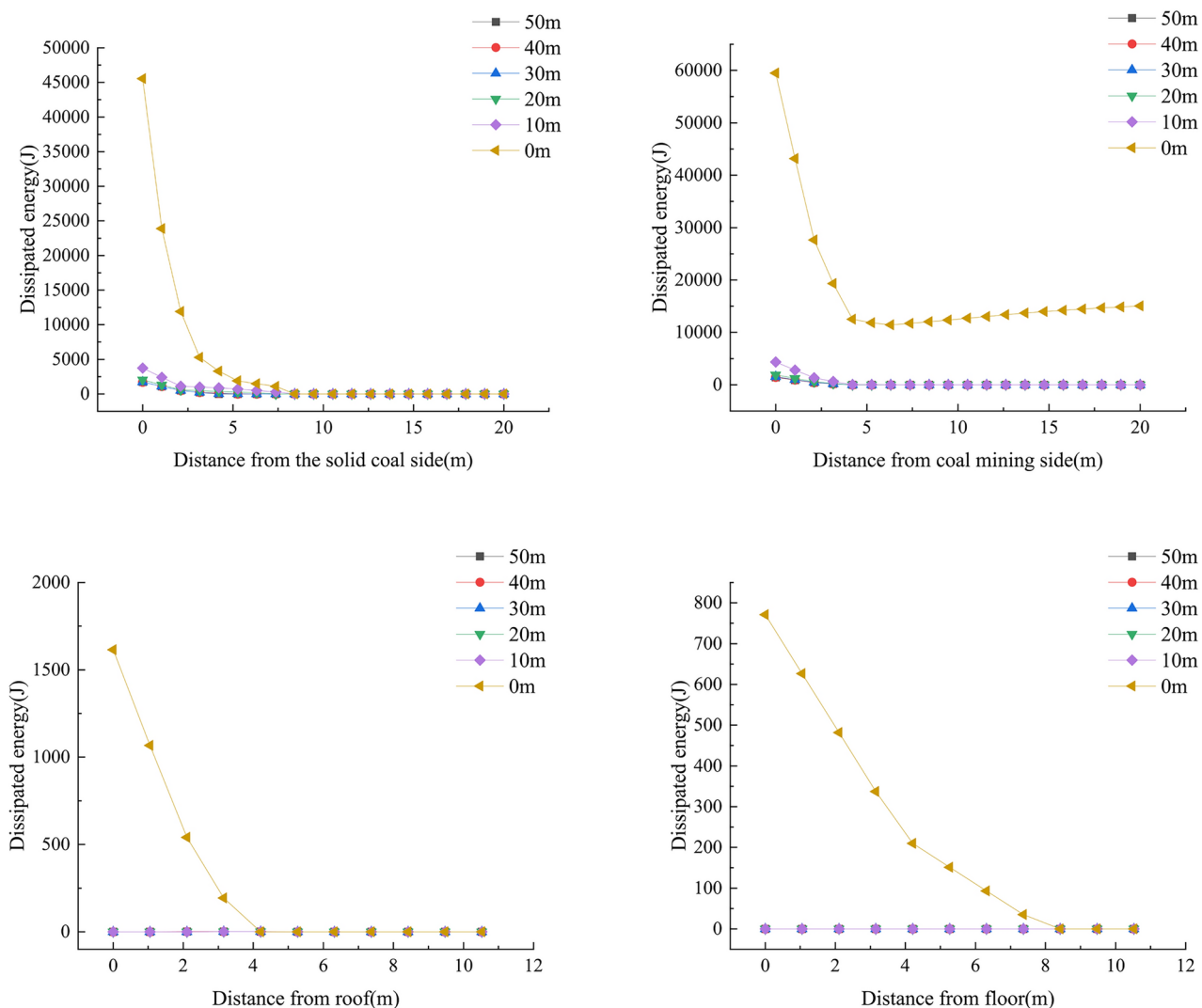


Fig. 4. Curve of dissipated energy distribution.

there must be some rock mass that consumes energy, some rock mass that supplies energy, and some rock mass that is far from the working face and is not affected by mining activities.

Based on the results of numerical simulation, the surrounding rock of the roadway is divided into three areas based on the boundary of the dissipated energy release range and the boundary of the elastic energy accumulation range. This paper will call them the energy consumption zone, the energy supply zone, and the unaffected zone, respectively. The division of energy zones of surrounding rock is shown in Fig. 7.

The area close to the working face is greatly affected by mining, and the coal mass in the area is affected by both the original rock stress and the mining stress. The energy accumulated by the surrounding rock of the roadway is in a state of release at this time, which is the energy consumption zone. The area slightly farther from the working face is still affected by mining, but its elastic energy accumulation is much greater than the release of dissipated energy. In terms of structure, it is not destroyed, and in terms of energy, it is the elastic energy transmitted to the energy consumption zone, which is the energy supply zone. The coal mass far from the working face is only affected by the original rock stress. The pressure in the area is small, and during the mining period, it is still in the elastic state in the stress-strain curve, which is the unaffected zone.

Identification of deformation and failure types

The causes of deformation and failure of surrounding rock in roadway are complex, there are many types of failure, and the hazards are great. In actual production, there is a lack of identification of deformation and failure of surrounding rock in roadway, which leads to a single type of roadway support, especially when facing impact instability and large deformation failure, it cannot ensure the stability of surrounding rock in roadway. Therefore, the identification of deformation and failure types of surrounding rock in roadway is of certain help to the stability of surrounding rock in mining roadway and the safe and efficient production of mining areas. This paper proposes the identification of deformation and failure types of surrounding rock in roadway from the perspective of energy level and energy release rate.

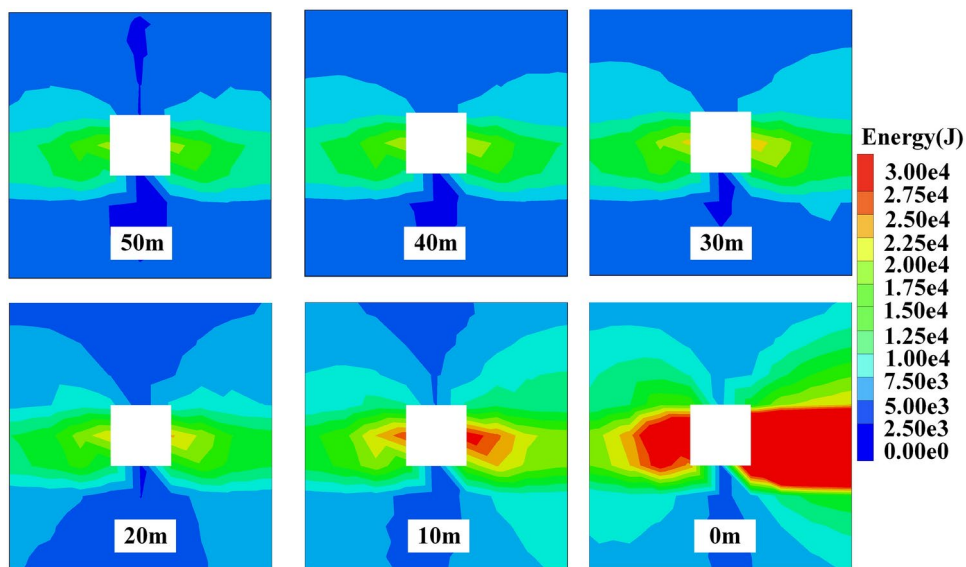


Fig. 5. Elastic energy distribution of surrounding rock.

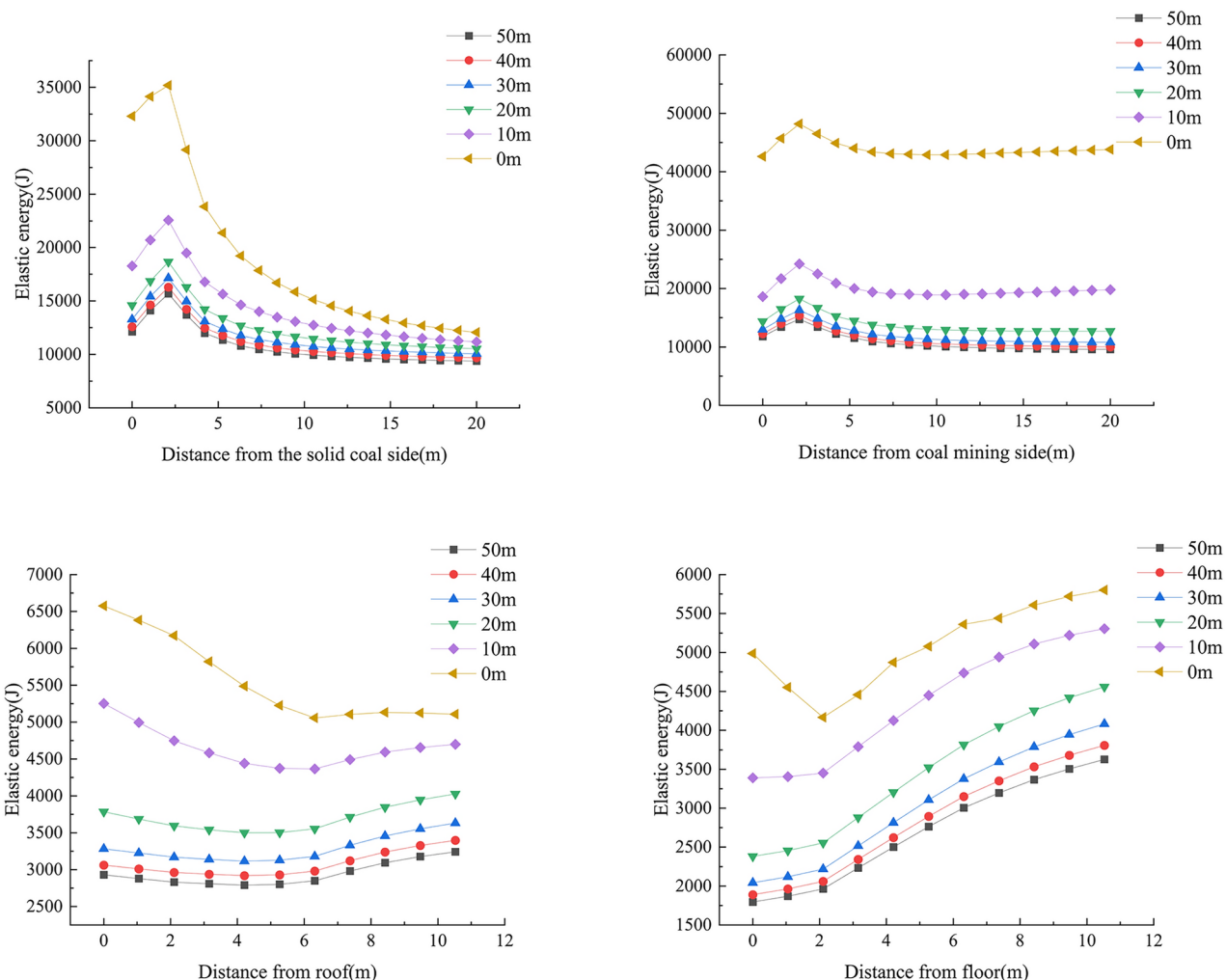


Fig. 6. Curve of elastic energy distribution.

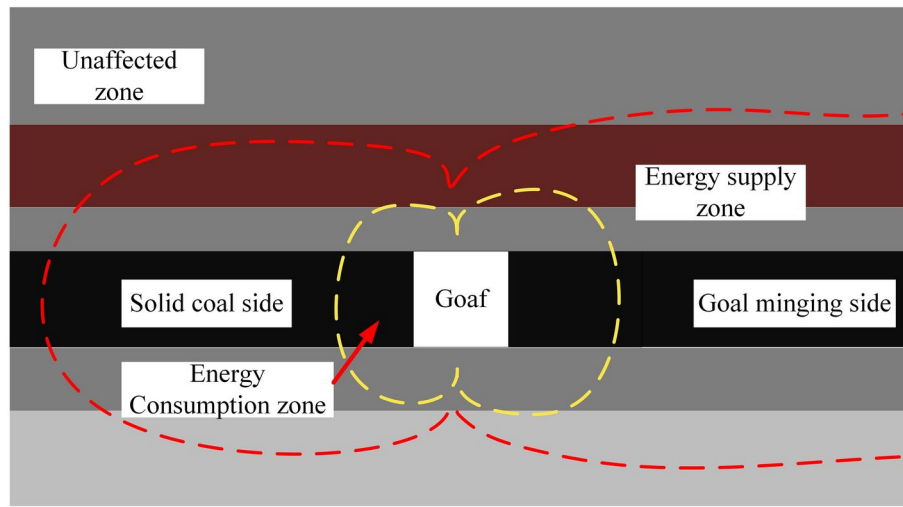


Fig. 7. Schematic diagram of energy partition of surrounding rock.

It is known from the stress-strain curve of rocks that when the external energy input to the rock reaches the peak energy threshold during the loading process of rocks, it enters the failure and instability stage.

The peak value energy threshold (U_s) of a single rock standard specimen during indoor experiments can be expressed as:

$$U_s = \int_0^{\varepsilon_s} \sigma d\varepsilon \quad (1)$$

The energy (U_t) accumulated by the in-situ rock layer at any time $t_1 - t_2$ can be expressed as:

$$U_t = \int_{\varepsilon_1}^{\varepsilon_2} \int_{t_1}^{t_2} \sigma_t d\varepsilon dt \quad (2)$$

The energy (U_0) accumulated by the original rock stress can be expressed as:

$$U_0 = \frac{\sigma_0^2}{2E} \quad (3)$$

The energy (U_d) generated due to different dynamic loads during the mining process can be expressed as:

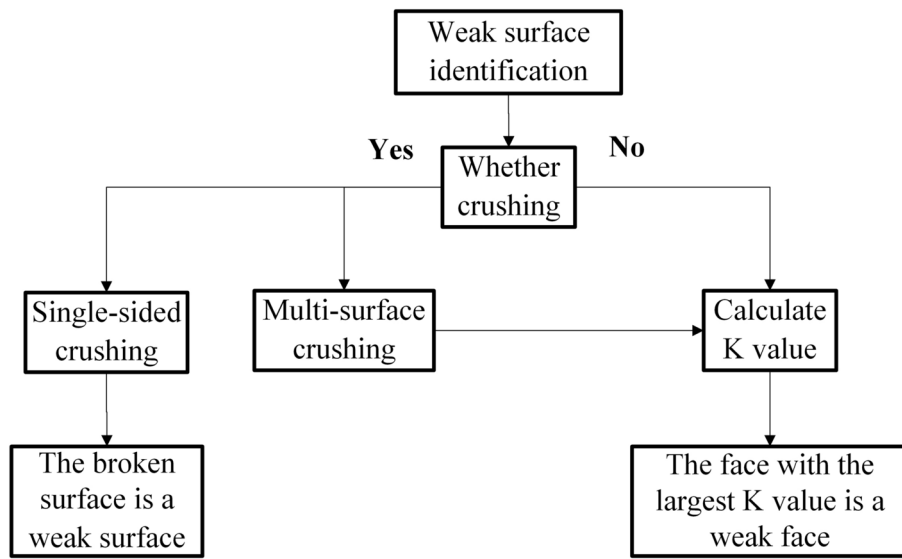
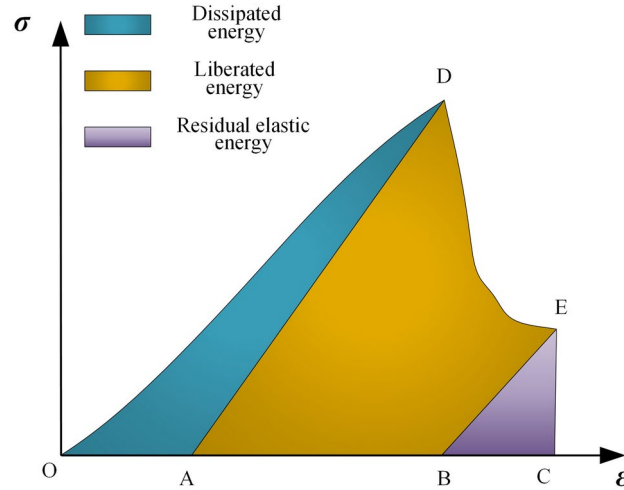
$$U_d = \sum_{i=1}^n U_i X_i^{-\alpha_i} \quad (4)$$

The ratio of the total energy value that the rock layer currently bears to the peak energy threshold is defined as the energy level identification coefficient K . When $K \geq 1$, it indicates that the total energy value currently borne by the rock layer has reached or exceeded the peak energy threshold, and the roadway will become unstable. When $K < 1$, it indicates that the total energy value currently borne by the rock layer has not reached the peak energy threshold, and the roadway will not become unstable.

$$K = \frac{\int_{\varepsilon_1}^{\varepsilon_2} \int_{t_1}^{t_2} \sigma_t d\varepsilon dt + \frac{\sigma_0^2}{2E} + \sum_{i=1}^n U_i X_i^{-\alpha_i}}{\int_0^{\varepsilon_s} \sigma d\varepsilon} \quad (5)$$

where ε_s is the strain corresponding to the failure peak stress; σ_t is the stress at time t ; σ_0 is the original rock stress; E is the elastic modulus; U_i is the energy released by different dynamic loads at the source; X_i is the distance of different sources from the roadway; and α_i is the energy propagation attenuation index of different dynamic loads in the coal-rock medium.

When the roadway undergoes deformation and failure, the elastic energy accumulated in the surrounding rock of the roadway is released and propagated to the weak face, which first fails, leading to the overall instability of the mining roadway. Therefore, it is necessary to identify the weak face in advance for the control of mining roadway.¹⁸ The peak energy threshold of the surrounding rock of the roadway will not change due to the external environment before failure. From Eq. (5), it can be concluded that the larger the K value, the greater the energy currently borne by the surrounding rock of the roadway, the lower the ability of the surrounding rock of the

**Fig. 8.** Flowchart for weak face identification.**Fig. 9.** The energy evolution characteristics of pre-peak and post-peak stages.²⁰

roadway to resist instability risk, and the more likely it is to become unstable. Therefore, K can be used to identify the weak faces of deformation and failure, and the identification process is shown in Fig. 8.

Roadway deformation and failure are manifestations of the magnitude and release rate of energy on weak face within the roadway. For the surrounding rock mass of the roadway, the type of failure can be identified by the evolution of energy during the failure process. By analyzing the relationship between the total energy, elastic strain energy, and the dissipated energy required for plastic deformation based on the complete stress-strain curve of rocks, the release rate of accumulated elastic energy is taken as one of the criteria for identifying the type of deformation and failure.¹⁹

As shown in Fig. 9, area S_{ODA} represents the dissipated energy required for fracturing and plastic deformation, area S_{ABD} represents the elastic energy stored during the loading process. Area S_{ABED} is the energy released when the coal-rock fails, and area S_{BCE} is the residual elastic energy after failure.

$$S_{ABD} = \frac{\sigma_s^2}{2E} \quad (6)$$

$$S_{BCE} = \frac{\sigma_r^2}{2E_r} \quad (7)$$

$$S_{BCED} = \int_{\varepsilon_D}^{\varepsilon_E} \sigma d\varepsilon \quad (8)$$

$$S_{ABED} = \frac{\sigma_s^2}{2E} + \int_{\varepsilon_d}^{\varepsilon_r} \sigma d\varepsilon - \frac{\sigma_r^2}{2E_r} = \frac{2EE_r \int_{\varepsilon_D}^{\varepsilon_r} \sigma d\varepsilon + E_r \sigma_s^2 - E \sigma_r^2}{2EE_r} \quad (9)$$

where σ_r is the residual stress; E_r is the elastic modulus after failure; ε_E is the strain at point E ; ε_D is the strain at point D .

The rate of energy release when the surrounding rock of the roadway undergoes deformation and failure is V_1 ,

$$V_1 = \frac{2EE_r \int_{\varepsilon_D}^{\varepsilon_r} \sigma d\varepsilon + E_r \sigma_s^2 - E \sigma_r^2}{2\Delta T_1 EE_r} \quad (10)$$

where ΔT_1 is the time at which deformation and failure occur in the surrounding rock of the roadway.

Assuming that the release speed of the peak energy threshold of the roadway instability is V_2 ,

$$V_2 = \frac{\int_0^{\varepsilon_s} \sigma d\varepsilon}{\Delta T_2} \quad (11)$$

where ΔT_2 is the release time of the peak energy threshold of the roadway instability.

$$V = \frac{2EE_r \Delta T_2 \int_{\varepsilon_D}^{\varepsilon_r} \sigma d\varepsilon + \Delta T_2 E_r \sigma_s^2 - \Delta T_2 E \sigma_r^2}{2\Delta T_1 EE_r \int_0^{\varepsilon_s} \sigma d\varepsilon} \quad (12)$$

The ratio of the rate of energy release when the surrounding rock of the roadway undergoes deformation and failure to the release speed of the peak energy threshold of roadway instability is defined as the rate identification coefficient V . If $V \geq 1$, impact instability occurs; if $V < 1$, large deformation failure occurs. The identification process is shown in Fig. 10.

Classified control technology

"Multi-Level pressure yielding" control technology

Traditional rigid support controls the large deformation of roadway by improving the stiffness and strength of the support structure.^{21,22} Although the rigid support scheme can suppress the deformation of the surrounding rock to a certain extent, when encountering soft surrounding rock, the force on the support system continues to increase, leading to harmful loosening and excessive displacement of the surrounding rock. With the continuous increase of surrounding rock deformation, the plastic zone continues to increase, eventually leading to the collapse of the roadway and causing huge losses.²³

Pressure yielding support is based on traditional rigid support, by adding some pressure yielding structures, allowing the surrounding rock to deform to a certain extent to release ground stress and reduce the pressure on the support structure, thus achieving stable control of the surrounding rock. Pressure yielding support only sets Pressure yielding structures at the end, and the pressure yielding amount is relatively small, so the control effect on the surrounding rock of large deformation roadway is still limited.

Therefore, aiming at the problem that traditional rigid support and pressure yielding support cannot well solve the control of surrounding rock of roadway at risk of large deformation, the "multi-level pressure yielding" control technology for surrounding rock of roadway at risk of large deformation is proposed.²⁴ Multi-level Pressure yielding support is further developed based on pressure yielding support. It can more finely control the deformation of the surrounding rock by setting multiple pressure yielding levels, adapting to the deformation

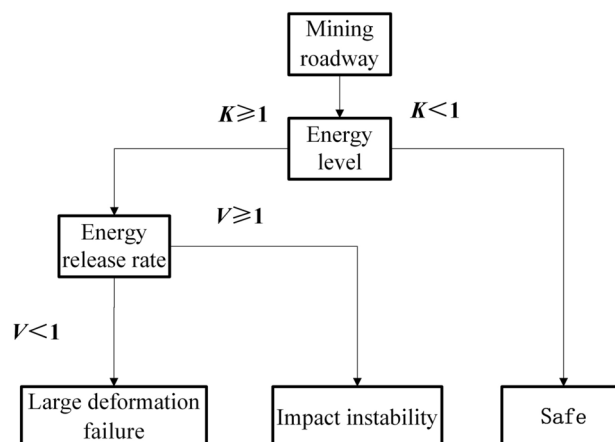


Fig. 10. Flowchart for deformation and failure type identification.

needs of different stages and degrees. The force characteristics of surrounding rock and structure under different support measures are shown in Fig. 11. Curve ① is traditional rigid support, and the support force f_3 bears is obviously higher than curves ② and ③. The force borne by the support structure is large, and stress concentration areas are prone to appear, which is not suitable for surrounding rock of roadway at risk of large deformation. Curve ② is pressure yielding support, which adds pressure yielding anchors and other pressure yielding structures based on traditional rigid support. By allowing a certain amount of displacement of the surrounding rock of the roadway, it has the ability to deform together with the surrounding rock, thus achieving the effect of releasing the stress of the surrounding rock. The support force it withstands is denoted as f_1 , and the yielding displacement is denoted as x_1 . Curve ③ is multi-level pressure yielding support, which continues to add pressure yielding components based on pressure yielding support, so that the pressure yielding amount of pressure yielding support is released in stages. The support force it withstands is denoted as f_2 . Its pressure yielding amount is the same as pressure yielding support, which is $(x_3 + x_4)$. Comparing curves ② and ③, curve ③ releases the total pressure yielding amount of curve ② by increasing the number of pressure yielding times, allowing it to intersect with the characteristic curve of the surrounding rock earlier and enter a stable state earlier. In summary, multi-level pressure yielding support bears less support resistance than rigid support, and the deformation of surrounding rock is reduced compared to pressure yielding roadway, and the surrounding rock enters a stable state earlier.²⁵ Multi-Level pressure yielding support can effectively control the surrounding rock of roadway at risk of large deformation.

"Relief-Support" control technology

It is known that when impact instability occurs, the coal mass will be instantly thrown out. As the surrounding rock energy continues to accumulate and release, it leads to the failure of the roadway sides from the surface to the inside. On the one hand, it is necessary to cut off the stress transmission path by relief, transferring the peak value of support pressure to a deeper part.²⁶ On the other hand, it is necessary to reinforce the shallow part of the roadway by strengthening support to prevent the broken coal mass in this area from being thrown out and causing impact instability.²⁷

Based on this, the "Relief-Support" control technology for surrounding rock of roadway at risk of impact instability is proposed, as shown in Fig. 12. On the one hand, technologies such as anchor bolts/cables, and grouting are used to support the energy release area of the coal roadway sides, reinforcing the broken area into a structure that can withstand pressure. On the other hand, technologies such as blasting to break the roof, large-diameter drilling pressure relief, and roof pre-splitting are used to relieve the coal mass or roof and floor, transferring the high-pressure peak area or energy accumulation area to the deep part of the sides, and keeping the high-energy accumulation area away from the mining space.²⁸ The "Relief-Support" control technology is shown in Fig. 13.

Engineering case studies

Transportation roadway of I0104,02 working face in Shuangma mine

Project overview

Shuangma mine is located about 60 km southeast of Lingwu City in the Ningxia. Currently, the main coal seams being mined are 4-2 and 4-3. The primary challenges faced are abnormal deformation and failure of the surrounding rock in the goaf of the I0104,02 working face caused by mining activities, as shown in Fig. 14. After identification, it belongs to large deformation failure.

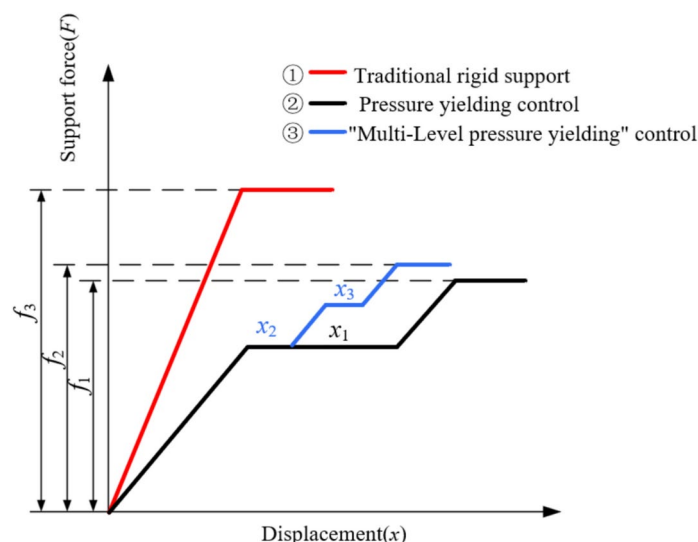


Fig. 11. The force characteristics of structure.

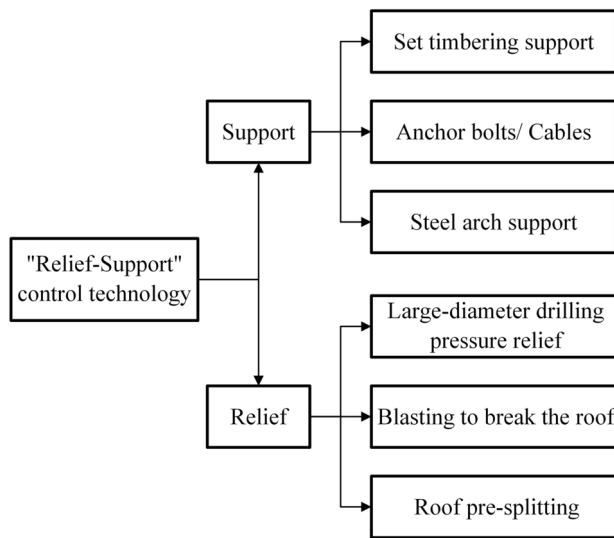


Fig. 12. Schematic diagram of "Relief-Support" control technology.

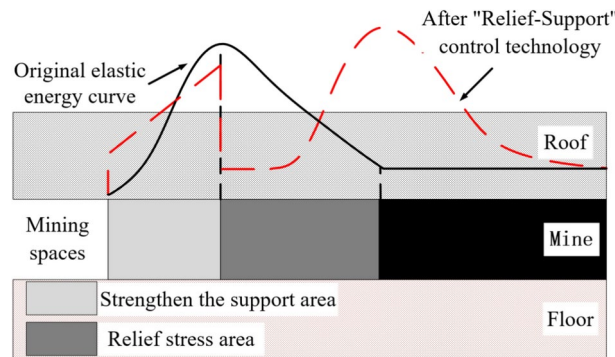


Fig. 13. Schematic diagram of "Relief-Support" control technology.

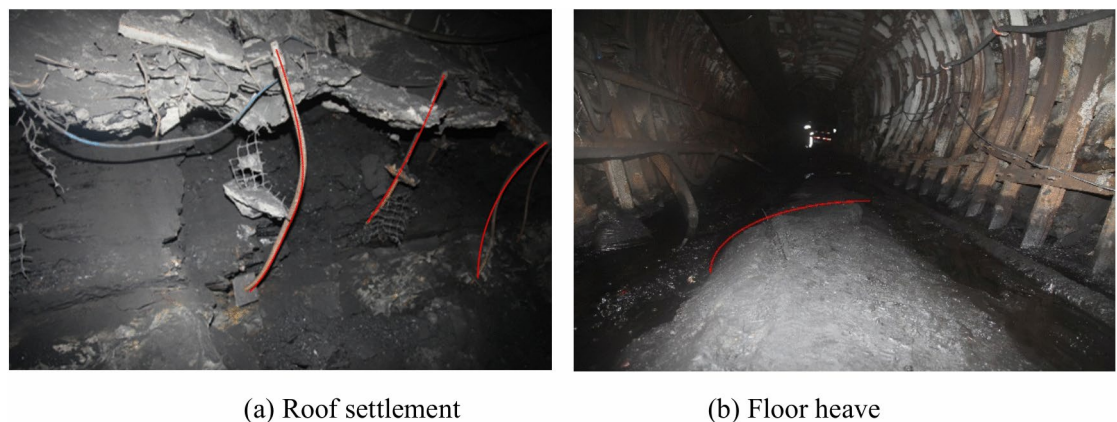


Fig. 14. Deformation and failure of surrounding rock of roadway.

"Multi-Level pressure yielding" control technology

Pressure yielding bolts+cable net support The top bolts are all pressure yielding bolts with a diameter of $\Phi 22 \times 2500$ mm, each with 2 rolls of MSCK2370 type resin anchoring agent, and the bolt spacing is 2500×1300 mm. The tray specification is a $150 \times 150 \times 12$ mm butterfly steel plates. The anchoring force of the bolts shall not be less than the standard value of the anchor bolt's yield strength, which is 130 kN.²⁹ The spacing

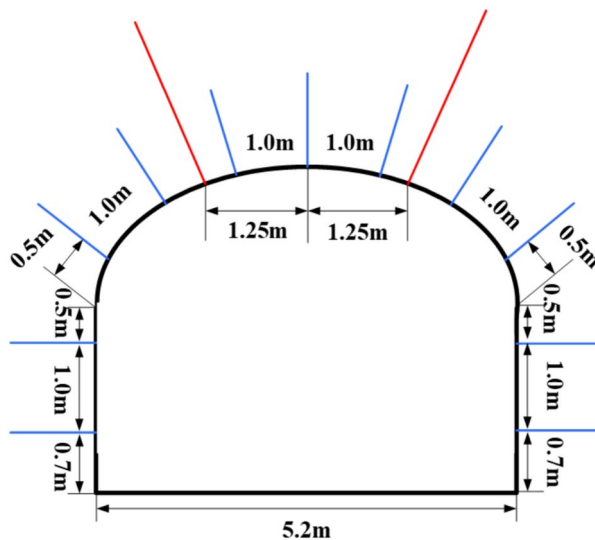


Fig. 15. Support cross-sectional diagram of I0104₃02 transportation roadway.

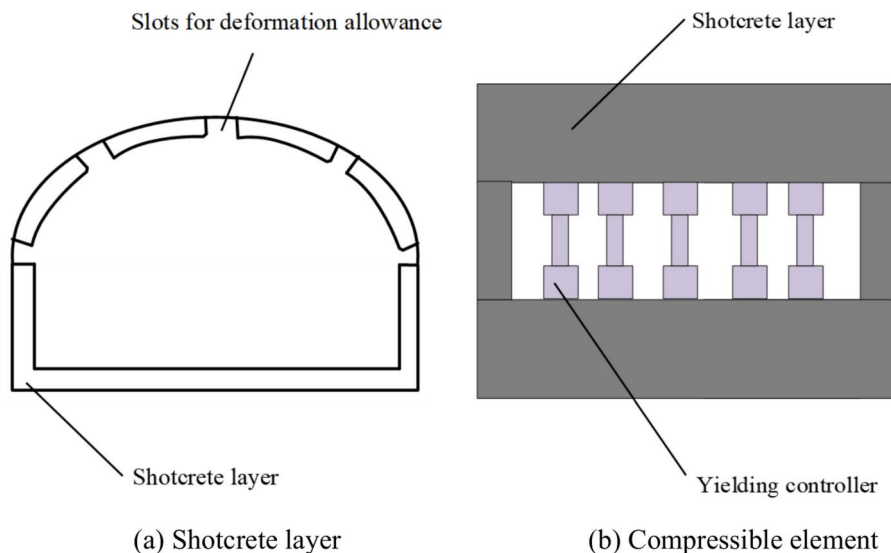


Fig. 16. Shotcrete layer diagram.

between the side anchor bolts is 1000×1300 mm. For the I0104₃02 working face transportation lane roof, anchor cables with a strength not lower than 356.43 kPa and a length not shorter than 4.06 m are selected, with a spacing of 1000 mm between the anchor cables and a row spacing of 2200 mm. Support cross-sectional diagram of I0104302 transportation roadway as shown in Fig. 15.

Shotcrete layer Surface treatment is carried out using spraying materials,³⁰ with a spraying thickness of 40–50 mm for the roof and both sides, a spraying strength of C20, and a spraying ratio of 1:2.2; the spraying material with a tensile strength of ≥ 3.0 MPa, an elongation rate of $\geq 20\%$, a bonding strength of ≥ 3.0 MPa, and a surface drying time of ≤ 60 min. Reserve deformation allowance slots during concrete spraying and install compression components in the slots. Shotcrete layer as shown in the Fig. 16.

Application effect analysis

This roadway surrounding rock monitoring technical plan mainly obtains on-site measured data such as roof separation and anchor/bolt force through monitoring methods such as anchor/bolt force gauges and roof separation instruments. A total of 4 observation stations are arranged in the I0104,02 working face transportation roadway, with 2 stations used to monitor the original support area (Area I) of the I0104,02 working face transportation roadway, and 2 stations used to monitor the "multi-level pressure yielding" control technology test area (Area II), as shown in Fig. 17.

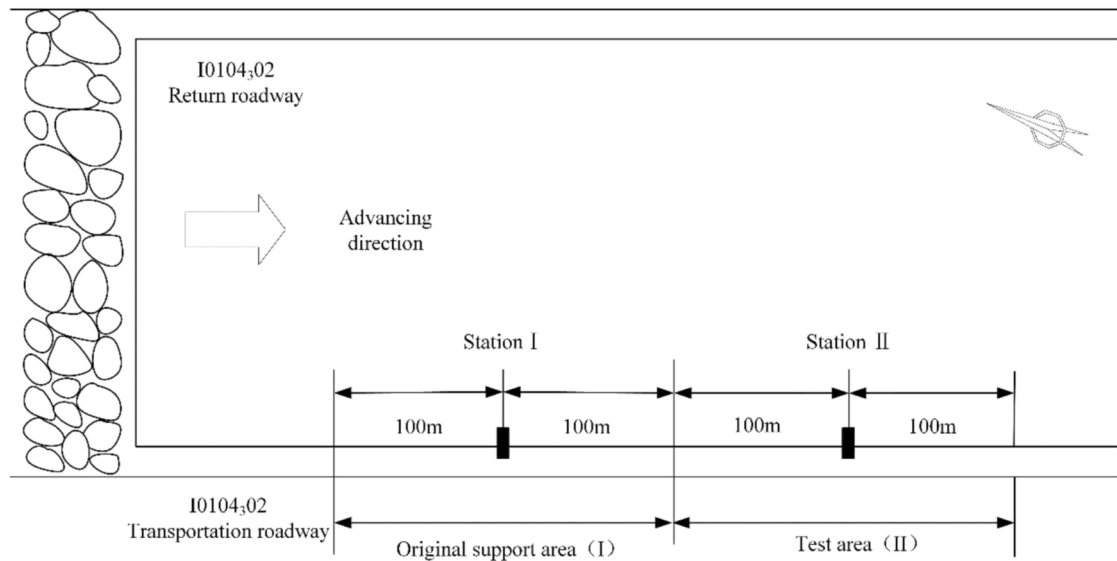


Fig. 17. Schematic diagram of monitoring station layout.

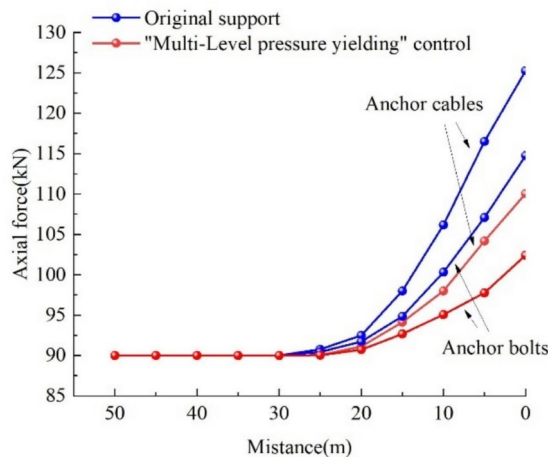


Fig. 18. Force monitoring diagram of bolts/ cables.

Anchor bolts/Cables force monitoring In order to obtain the force situation of anchor bolts/cables in the I0104₃02 transportation roadway and evaluate the support effect of the "multi-level pressure yielding" control technology,³¹ a anchor bolts/cables force gauge is used to monitor the roof of the I0104₃02 transportation roadway. The monitoring results of the cable force gauge are shown in Fig. 18.

The monitoring results from the bolt/cable load cells show that under the original support conditions, when the working face advanced to 30 m away from the monitoring station, the axial forces of the bolts/cables began to increase due to mining-induced stress. The axial forces reached their maximum values when the working face advanced to the monitoring station, with the bolt axial force at 117 kN and the cable axial force at 133 kN. After implementing the "multi-level pressure yielding" integrated control strategy, the axial forces of the bolts/cables started to increase when the working face advanced to 27 m from the monitoring station under mining-induced stress and similarly peaked at the monitoring station. The bolt axial force was 103 kN, representing a reduction compared to the original support scheme, and the cable axial force was 110 kN, also showing a decrease. The monitoring results indicate effective support performance.

Roof separation monitoring In order to obtain the roof separation situation of the support optimization plan in the I0104₃02 transportation roadway and evaluate the support effect of the "multi-level pressure yielding" control technology, a roof separation instrument is used to monitor the roof of the I0104₃02 transportation roadway. The monitoring results of the roof separation instrument are shown in Fig. 19.

The monitoring results from the roof separation instruments reveal that during the mining of the I0104₃02 working face, the relative displacement under the original support scheme continued to increase until stabilizing

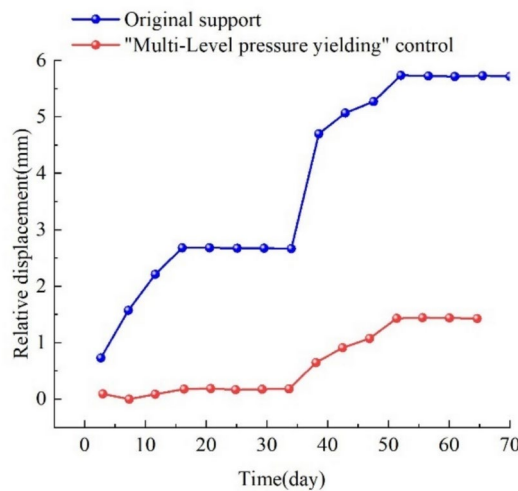


Fig. 19. Roof separation monitoring.

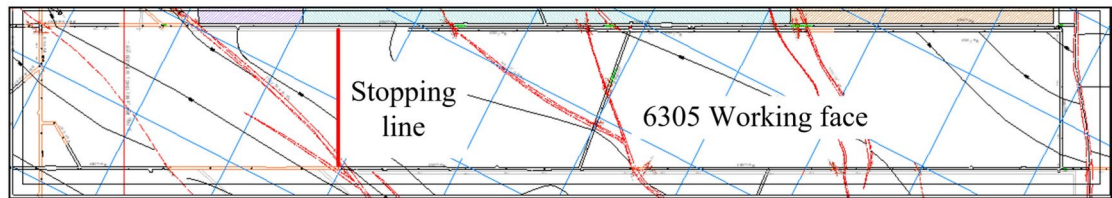


Fig. 20. Plan view of 6305 working face.

temporarily at 3 mm, indicating the development of fractures in the roadway roof due to concentrated stress from coal pillars. On day 35, the roof began to be affected by mining-induced stress, leading to a further increase in relative displacement until stabilization at 6 mm, demonstrating significant mining impact and progressive delamination of the roof. After implementing the "multi-level pressure yielding" integrated control, the relative displacement of the roadway roof showed minimal change during days 0–35, confirming effective control of roof delamination. On day 35, the relative displacement of roof delamination started to increase and stabilized at 1.5 mm, indicating the onset of mining-induced influence. Compared with the pre-control scenario, the relative displacement of roof delamination under the "unloading-support" strategy was reduced by 266%, with no significant delamination observed and intact shallow roof strata. The "multi-level pressure yielding" integrated control effectively protected the roof, demonstrating favorable support performance.

Based on the "multi-level pressure yielding" control design and on-site engineering practice, it is shown that:

- (1) After the "multi-level pressure yielding" control, the force on the anchor bolts/ cables in the I0104₃02 transportation roadway was reduced by 12.0% and 17.3%, respectively, and the stability of the surrounding rock of the roadway was enhanced.
- (2) The relative displacement of the roof separation instrument in the I0104₃02 transportation roadway was reduced by 266% compared to before the "multi-level pressure yielding" control, and the deformation and failure of the surrounding rock of the roadway were effectively controlled.

Intake roadway of 6305 working face in Xinjulong mine

Project overview

Xinjulong Coal Mine is one of the mines with serious impact pressure hazards,³² and the 6305 working face is a demonstration working face for impact prevention in the mine. After identification, it has the risk of impact instability. Its designed strike length is 1390 m, and the dip length is 260.6–265.5 m. The coal layer is the 3rd coal layer, with a small variation in coal thickness, 8.1–10 m in thickness, an average coal thickness of 9.08 m, and a coal layer dip angle of 0°–16°, with an average of 8°. The plan view of the 6305 working face is shown in Fig. 20.

"Relief-Support" control technology

Blasting to break the roof Dip blasting hole layout: 3 holes per group, spaced 7.5 m apart, with a hole diameter of 89 mm, drilled vertically down the side, with angles of 80°, 70°, and 50°, and hole depths of 51 m, 53 m, and 66 m, respectively, with charge weights of 75 kg, 78 kg, and 99 kg, respectively. Blast one group at a time.

Strike blasting hole layout: Arranged along the strike of the roadway, 2 strike blasting holes are arranged between two groups of dip blasting holes, with a hole spacing of 5m, an angle of 70°, and a hole depth of 50 m, with a charging amount of 75 kg.

Strengthened support Between the roof steel straps, 29# U-shaped anchor cable beams (one beam with three cables) are added, with the anchor cable beam being 4500 mm long, the hole spacing being 1800 mm, and the row spacing being 1000 mm with double bearing plates. The anchor cables use $\Phi 21.8 \times 6300-10300$ mm high-prestress steel strand, with an bond length of not less than 1500 mm and a pre-tightening force of not less than 200 kN. The side of the anchor cable beam is inclined 10°–30° towards the side.

The west side is supplemented with 2 U-type anchor cable beams (one beam with two cables), with a length of 2600 mm, hole spacing of 2000 mm, and row spacing of 2000×2000 mm. The anchor cables use $\Phi 21.8 \text{ mm} \times 8300$ mm steel strand anchor cables, with the lower hole position drilled vertically down the side. Permanent support cross-sectional diagram of 6305 intake airway as shown in Fig. 21.

Application effect analysis

This roadway surrounding rock monitoring technical plan mainly obtains on-site measured data of surrounding rock damage and microseismic events through monitoring methods such as microseismic monitoring and drilling debris method.³³ A total of 2 observation stations are arranged in the 6305 working face intake roadway, with 1 station used to monitor the original support area (Area I) of the 6305 working face intake roadway, and 1 station used to monitor the "Relief-Support" control technology test area (Area II), as shown in Fig. 22.

Microseismic analysis By counting the number and energy size of microseismic events in the 6305 working face intake roadway, the number and proportion of microseismic events with high energy before and after the "Relief-Support" control are obtained.

As shown in Fig. 23, before the "Relief-Support" control, microseismic events with energy greater than 10^3 J account for 22.77% of the total number of microseismic events, and events with energy exceeding 4×10^4 J have occurred. Compared with before the "Relief-Support" control, the microseismic energy fluctuation curve is more uneven, and high energy events occur more frequently. After the "Relief-Support" control, microseismic events greater than 10^3 J account for 15.56% of the total microseismic events, a decrease of 7.21%. From the "Relief-Support" control point onwards, the overall microseismic energy fluctuation is more stable, and the frequency of high-energy events is reduced.

Drill cuttings analysis By organizing the results of the drill cuttings monitoring in the 6305 working face intake roadway, analyses were conducted at locations 10 m and 20 m ahead of the measuring station, and 10 m and 20 m behind the measuring station, before and after the "Relief-Support" control. The coal powder quantity before and after the "Relief-Support" control is shown in Tables 2 and 3.

As shown in Fig. 24, after the implementation of the "Relief-Support" control measures, the amount of coal cuttings has decreased compared to before the "Relief-Support" control. The drilling powder rate index, which indicates the risk of impact danger at the workplace, has also significantly decreased, indicating a clear reduction in the risk of impact danger in this area.^{34,35}

Based on the "Relief-Support" control design and on-site engineering practice, it is shown that:

(1) After the "Relief-Support" control, the proportion of microseismic events greater than 10^3 J decreased by 7.21%, and the overall microseismic energy fluctuation is more stable, with a reduced frequency of high-energy events.

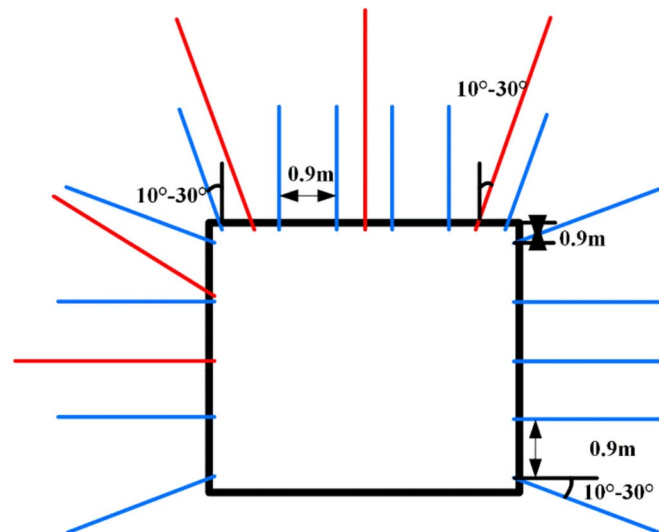


Fig. 21. Permanent support cross-sectional diagram of 6305 intake airway.

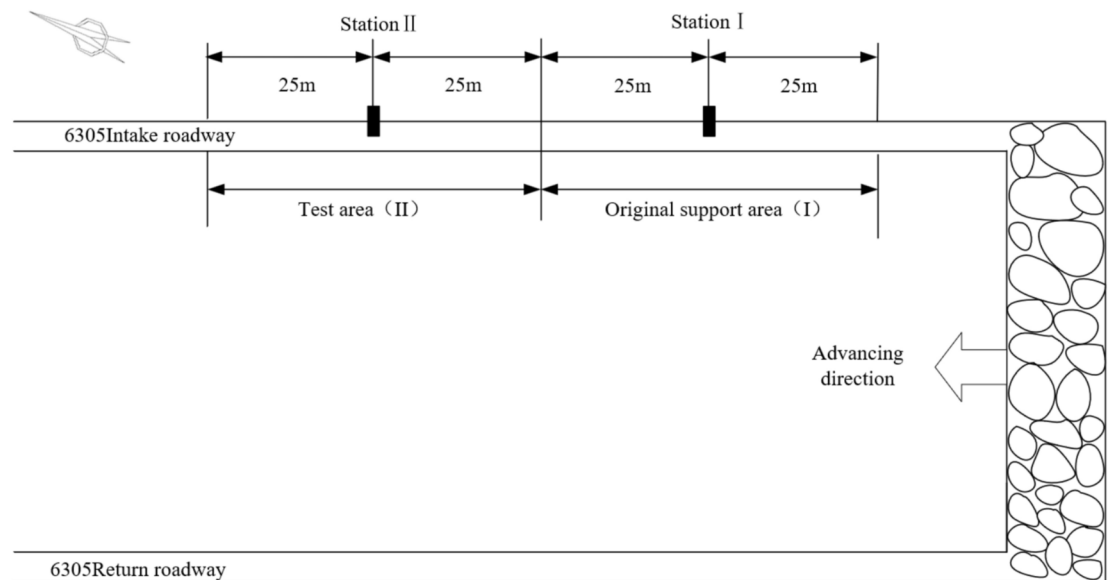


Fig. 22. Schematic diagram of monitoring station layout.

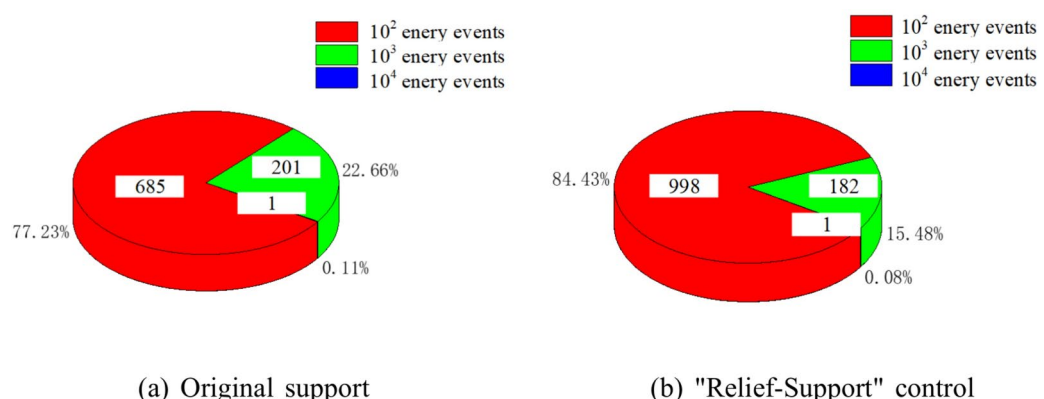


Fig. 23. Comparison of high energy microseismic events (a) Original support (b) "Relief-Support" control.

Location	Dynamic effects	Coal quantity (kg)														
		1	2	3	4	5	6	7	8	9	10	11	12	13	14	15
Before station I 20 m	Not	1.0	2.0	1.9	2.0	1.6	2.4	2.9	2.0	3.4	1.5	2.6	1.7	3.7	2.4	2.6
Before station I 10 m	Not	1.2	1.4	2.0	1.5	2.5	1.5	2.7	2.1	2.5	4.3	2.4	1.5	2.0	1.7	3.2
After station I 10 m	Not	1.2	1.8	1.9	2.0	2.6	2.5	3.1	3.7	3.5	2.3	2.5	2.6	2.6	3.0	3.0
After station I 20 m	Not	1.7	1.6	2.0	2.4	2.1	2.9	1.7	2.6	2.9	2.0	2.4	2.0	3.7	1.9	1.1

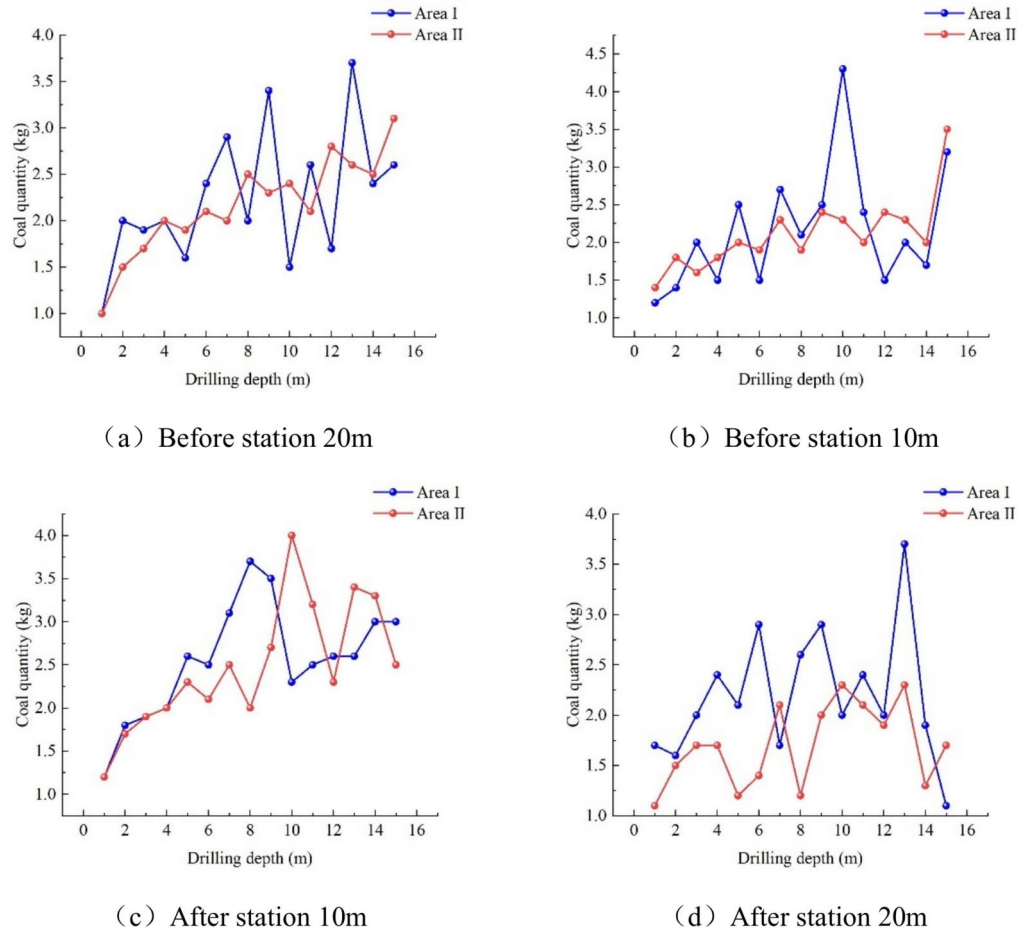
Table 2. Drill cuttings monitoring before "Relief-Support" control.

(2) After the "Relief-Support" control, the dynamic effect of the workplace's impact danger showed no change, but the drilling powder rate index, which indicates the risk of impact danger, decreased, indicating a clear reduction in the risk of impact danger in this area.

Conclusion

1. Based on numerical simulation, the advance influence range of mining roadway is approximately 30 m. The energy influence range and value at both sides of the roadway gradually increase with the mining of the working face, reaching the limit at 10 m ahead of monitoring line. Then it spreads from both sides towards

Location	Dynamic effects	Coal quantity (kg)														
		1	2	3	4	5	6	7	8	9	10	11	12	13	14	15
Before station II 20 m	Not	1	1.5	1.7	2	1.9	2.1	2	2.5	2.3	2.4	2.1	2.8	2.6	2.5	3.1
Before station II 10 m	Not	1.4	1.8	1.6	1.8	2	1.9	2.3	1.9	2.4	2.3	2	2.4	2.3	2	3.5
After station II 10 m	Not	1.2	1.7	1.9	2	2.3	2.1	2.5	2	2.7	4	3.2	2.3	3.4	3.3	2.5
After station II 20 m	Not	1.1	1.5	1.7	1.7	1.2	1.4	2.1	1.2	2	2.3	2.1	1.9	2.3	1.3	1.7

Table 3. Drill cuttings monitoring after "Relief-Support" control.**Fig. 24.** Comparison curve of coal powder quantity.

the roof and floor and reaches its maximum in face end, forming a butterfly-shaped dissipation area and a trapezoidal elastic area. The surrounding rock of the roadway is divided into energy consumption zone, energy supply zone, and unaffected zone based on the range

2. From the aspects of energy level and energy release rate, a method for identifying the types of surrounding rock deformation and failure is proposed. When the energy level identification coefficient $K \geq 1$ and the energy rate identification coefficient $V \geq 1$, the surrounding rock of the roadway undergoes impact instability; when the energy rate identification coefficient $V < 1$, the surrounding rock of the roadway undergoes large deformation failure.
3. A "Multi-Level pressure yielding" control technology for surrounding rock of roadway at risk of large deformation was proposed and applied in Shuangma Mine. On-site monitoring results show that after adopting the control technology, the force on anchor bolts/cables was reduced by 12.0% and 17.3%, respectively, and the relative displacement of the roof separation instrument was reduced by 266%. The deformation and failure of surrounding rock were effectively controlled.
4. An "Relief-Support" control technology for surrounding rock of roadway at risk of impact instability was proposed and applied in Xinjulong. On-site monitoring results show that after adopting the control technology, the proportion of large energy microseismic events decreased by 7.21%, and the drilling powder rate index decreased, reducing the risk of impact instability in the roadway.

Data availability

The original contributions presented in the study are included in the article material. Further inquiries can be directed to the corresponding author. The data used to support the findings of this research are included within the paper.

Received: 21 November 2024; Accepted: 11 April 2025

Published online: 30 April 2025

References

1. Qian, M. G., Shi, P. W. & Xu, J. L. *Mine pressure and strata control* 84–99 (China University of Mining and Technology Press, 2003).
2. Xie, H. et al. Study on the mechanical properties and mechanical response of coal mining at 1000 m or deeper. *Rock Mech. Rock Eng.* **52**(5), 1475–1490 (2019).
3. Zuo, J. P., Wang, J. T. & Jiang, Y. Q. Macro/meso failure behavior of surrounding rock in deep roadway and its control technology. *Int. J. Coal Sci. Technol.* **6**(3), 301–319 (2019).
4. Hermann, K. *Tunnel and shaft statics* 58–59 (Shanghai Scientific & Technical Publishers, 1980).
5. Wang, W. J. & Hou, C. J. Study of mechanical principle of floor heave of roadway driving along next goaf in fully mechanized sub-level caving face. *J. Coal Sci. Eng. (China)* **1**, 13–17 (2001).
6. Gao, L. et al. Stress distribution characteristics of the surrounding rock of the gob-side coal-rock roadway in a gently inclined coal seam under the influence of excavation and mining disturbance based on infrared detection. *Int. J. Geomech.* <https://doi.org/10.1061/IJGNALGMENG-8571> (2023).
7. Hong, R. C., Ping, C. & Hang, L. A kind of control technology for squeezing failure in deep roadways: A case study. *Geomat. Nat. Haz. Risk* **8**(2), 1715–1729 (2017).
8. Yang, S. et al. Instability mechanism and stability control of gob-side entry in a deep mine: a case study. *Bull. Eng. Geol. Environ.* <https://doi.org/10.1007/s10064-023-03362-6> (2023).
9. Jing, W. et al. Mechanical effects and existing problems analysis of anchor frame combination supporting structure. *Appl. Mech. Mater.* **3147**(548–549), 422–427 (2014).
10. Xu, Q. Y. et al. The use of surrounding rock loosening circle theory combined with elastic-plastic mechanics calculation method and depth learning in roadway support. *PLoS ONE* **15**(7), e0234071 (2020).
11. Daemen, J. J. K. *Tunnel support loading caused by rock failure* (University of Nevada, 1975).
12. Zhang, D. et al. Research on selection of preliminary support for tunnel in high ground-stress soft rock based on surrounding rock-support characteristic curve theory. *Chin. Civil Eng. J.* **48**(1), 139–148 (2015).
13. Zhao, Y., Liu, J. & Tian, S. Experimental study of mechanical characteristics of support system for weak surrounding rock of deep tunnels. *Chin. J. Rock Mech. Eng.* **30**(8), 1663–1670 (2011).
14. Tan, Y. L. et al. Numerical investigation of failure evolution for the surrounding rock of a super-large section chamber group in a deep coal mine. *Energy Sci. Eng.* **7**(6), 3124–3146 (2019).
15. Liu, X. S. et al. Damage constitutive model based on energy dissipation for intact rock subjected to cyclic loading. *Int. J. Rock Mech. Min. Sci.* **85**, 27–32 (2016).
16. Zhang, J. et al. Study on roadway roof deformation and coal pillar energy accumulation instability. *Sci. Rep.* **14**(1), 27603–27603 (2024).
17. Randriantsoa, A. N. A. et al. Research and development of a new combination of piezo-thermoelectric energy harvester systems from roadways. *Eng. Res. Expr.* **6**, 1 (2024).
18. Zheng, K. et al. A computational method for tunnel energy evolution in strain-softening rock mass during excavation unloading based on triaxial stress paths. *Comput. Geotech.* **169**, 106212 (2024).
19. Wang, Y. et al. Deformation mechanism and control technology of gob-side entry retaining with roadside backfilling: A numerical analysis and field investigation. *Geomech. Geophys. Geo-Energy Geo-Res.* **10**(1), 175–175 (2024).
20. Kivi, I., Ameri, M. & Molladavoodi, H. Shale brittleness evaluation based on energy balance analysis of stress-strain curves. *J. Petrol. Sci. Eng.* **167**, 1–19 (2018).
21. Onur, V. et al. An energy-based quantitative coal burst proneness rating system for development roadways. *Geomech. Geophys. Geo-Energy Geo-Resour.* **9**, 1 (2023).
22. Liu, X. S. et al. Roof fracture and front abutment stress evolution of large mining height coal face with weak overburden under goaf. *Earth Environ. Sci.* **570**, 052010 (2020).
23. Liu, X. S. et al. Failure evolution and instability mechanism of surrounding rock for close-distance chambers with super-large section in deep coal mines. *Int. J. Geomech.* **21**(5), 04021049 (2021).
24. Wu, K. et al. The deformation coordination-dominated design of yielding supports applied in large deformation tunnels. *Acta Geotech.* **19**(5), 2499–2513 (2024).
25. Fan, D. Y. et al. Energy mechanism of bolt supporting effect to fissured rock under static and dynamic loads in deep coal mines. *Int. J. Min. Sci. Technol.* <https://doi.org/10.1016/j.ijmst.2024.03.001> (2024).
26. Zhao, J. H. et al. Mine water inrush characteristics based on RQD index of rock mass and multiple types of water channels. *Geomech. Eng.* **38**(3), 215–229 (2024).
27. Liu, X. S. et al. New detecting method on the connecting fractured zone above the coal face and a case study. *Rock Mech. Rock Eng.* **54**, 4379–4391 (2021).
28. Ren, F. et al. Effects of pressure relief holes on coal burst: Insights from true-triaxial unloading tests. *J. Rock Mech. Geotech. Eng.* **16**(9), 3378–3394 (2024).
29. Cai, T. et al. Study on the instability mechanism and control technology of narrow coal pillar in double-roadway layout of Changping mine. *Sci. Rep.* **14**(1), 16676–16676 (2024).
30. Zhang, Z. G. et al. In Situ tests comparing the support effects of thin spray-on liner and shotcrete on a roadway subjected to blasting. *Rock Mech. Rock Eng.* **57**(3), 1669–1693 (2023).
31. Chen, D. et al. Study on the mechanism of progressive instability of special-shaped coal pillar and the stability control of roadway under the influence of mining. *Rock Mech. Rock Eng.* **57**(8), 6461–6483 (2024).
32. Tan, Y. L. et al. Failure prediction from crack evolution and acoustic emission characteristics of coal-rock sandwich composite samples under uniaxial compression. *Bull. Eng. Geol. Environ.* **81**, 200 (2022).
33. Liu, X. S. et al. Similar simulation study on the deformation and failure of surrounding rock of a large section chamber group under dynamic loading. *Int. J. Min. Sci. Technol.* **31**, 495–505 (2021).
34. Fatemeh, S. et al. Numerical modelling of coal and gas outburst initiation using energy balance principles. *Fuel* **334**, P1 (2023).
35. Onur, V. et al. Numerical investigation of impacts of geological faults on coal burst proneness during roadway excavation. *Bull. Eng. Geol. Env.* **81**, 1 (2021).

Acknowledgements

This study was financially supported by the National Natural Science Foundation of China (Nos. 52374218 and

52174122), Excellent Youth Fund of Shandong Natural Science Foundation (No. ZR2022YQ49). Taishan Scholar in Shandong Province (tsqn202211150).

Author contributions

Xuesheng Liu: Conceptualization, Project Administration and Funding Acquisition; Yu Zhang: Writing-Original Draft Preparation, Data Curation and Methodology; Yudong Gao: Validation, Formal Analysis and Resources; Yongqiang Zhao: Writing-Review & Editing and Investigation; Hongxi Pei: Visualization; Zhihan Shi: Software; Deyuan Fan: Supervision.

Declarations

Competing interests

The authors declare no competing interests.

Additional information

Correspondence and requests for materials should be addressed to Y.Z. or D.F.

Reprints and permissions information is available at www.nature.com/reprints.

Publisher's note Springer Nature remains neutral with regard to jurisdictional claims in published maps and institutional affiliations.

Open Access This article is licensed under a Creative Commons Attribution 4.0 International License, which permits use, sharing, adaptation, distribution and reproduction in any medium or format, as long as you give appropriate credit to the original author(s) and the source, provide a link to the Creative Commons licence, and indicate if changes were made. The images or other third party material in this article are included in the article's Creative Commons licence, unless indicated otherwise in a credit line to the material. If material is not included in the article's Creative Commons licence and your intended use is not permitted by statutory regulation or exceeds the permitted use, you will need to obtain permission directly from the copyright holder. To view a copy of this licence, visit <http://creativecommons.org/licenses/by/4.0/>.

© The Author(s) 2025